The Journal of Chemical Physics

Unconventional S_N2 retention pathways induced by complex formation: High-level dynamics investigation of the NH_2^- + CH_3I polyatomic reaction

Cite as: J. Chem. Phys. **156**, 184306 (2022); https://doi.org/10.1063/5.0091789
Submitted: 17 March 2022 • Accepted: 15 April 2022 • Accepted Manuscript Online: 18 April 2022 • Published Online: 12 May 2022

Domonkos A. Tasi and Gábor Czakó

AIP Publishing

The Journal of Chemical Physics ARTICLE scitation.org/journal/jcp

Unconventional S_N2 retention pathways induced by complex formation: High-level dynamics investigation of the NH_2^- + CH_3I polyatomic reaction

Cite as: J. Chem. Phys. 156, 184306 (2022); doi: 10.1063/5.0091789
Submitted: 17 March 2022 • Accepted: 15 April 2022 •
Published Online: 12 May 2022

Domonkos A. Tasi[a] and Gábor Czakó[a]

AFFILIATIONS

MTA-SZTE Lendület Computational Reaction Dynamics Research Group, Interdisciplinary Excellence Centre and Department of Physical Chemistry and Materials Science, Institute of Chemistry, University of Szeged, Rerrich Béla tér 1, Szeged H-6720, Hungary

[a]Authors to whom correspondence should be addressed: dtasi@chem.u-szeged.hu and gczako@chem.u-szeged.hu

ABSTRACT

Investigations on the dynamics of chemical reactions have been a hot topic for experimental and theoretical studies over the last few decades. Here, we carry out the first high-level dynamical characterization for the polyatom–polyatom reaction between NH_2^- and CH_3I. A global analytical potential energy surface is developed to describe the possible pathways with the quasi-classical trajectory method at several collision energies. In addition to S_N2 and proton abstraction, a significant iodine abstraction is identified, leading to the CH_3 + $[NH_2\cdots I]^-$ products. For S_N2, our computations reveal an indirect character as well, promoting the formation of $[CH_3\cdots NH_2]$ complexes. Two novel dominant S_N2 retention pathways are uncovered induced by the rotation of the CH_3 fragment in these latter $[CH_3\cdots NH_2]$ complexes. Moreover, these uncommon routes turn out to be the most dominant retention paths for the NH_2^- + CH_3I S_N2 reaction.

INTRODUCTION

Bimolecular nucleophilic substitution (S_N2) is a well-known stereo-specific reaction type, and it has been in the center of chemical interest since the middle of the 20th century.[1–17] In a schematic X^- + CH_3Y → CH_3X + Y^- S_N2 reaction, Walden inversion occurs via a pre-reaction complex ($X^-\cdots CH_3Y$) and/or a hydrogen-bonded complex ($X^-\cdots HCH_2Y$) followed by a central barrier $[X\cdots CH_3\cdots Y]^-$, and then, in most cases, a post-reaction ($XCH_3\cdots Y^-$) complex is formed. The front-side attack mechanism, where the attacking X^- nucleophile approaches from the Y-side of CH_3Y, instead of the back-side of the methyl group, results in retention by a high-energy $[XYCH_3]^-$ transition state. However, in the past two decades, it was unveiled that the above-described classical picture of S_N2 reactions is much more complex: Various other mechanisms can be found such as rebound, stripping, ion-dipole complex formation, hydrogen-bonded complex formation, front-side complex formation, and roundabout.[18] Note that, in our studies, these pathways are subsumed under the back-side attack Walden-inversion mechanism.[19] In 2015, our dynamics investigation on the F^- + CH_3Cl reaction revealed that besides front-side attack, retention can also take place along a lower-energy pathway.[20] This so-called double-inversion mechanism starts with a proton-abstraction induced inversion followed by a Walden inversion via the traditional $[X\cdots CH_3\cdots Y]^-$ transitional state. Moreover, in most cases, proton abstraction can occur, resulting in the HX + CH_2Y^- products.

Moving beyond the traditional six-atomic S_N2 reactions between halide ions and methyl halides, several investigations were carried out on the OH^- + CH_3Y [Y = F, Cl, Br, I] seven-atomic systems.[21–31] For Y = F, dynamics simulations were performed by Hase and co-workers, and it was found that 90% of the trajectories did not follow the intrinsic reaction coordinate avoiding the hydrogen-bonded global minimum ($CH_3OH\cdots F^-$) of the potential

energy surface (PES).[21] Furthermore, recent dynamics studies revealed that the importance of this latter minimum is not negligible; in some cases, the fluoride ion removes the proton from the hydroxyl group leading to the unexpected HF + CH_3O^- products.[32,33] The most studied reaction is OH^- + CH_3I: The stationary-point characterization using density functional theory calculations and the dynamics simulations were performed by the Hase group, and the experimental investigations were implemented by the groups of Viggiano and Wester.[28,29,34,35] The influence of the water molecules on the dynamics of the latter reaction was also studied;[7] moreover, Xie and co-workers examined the solvent effect on the front-side complex mechanism.[36] In 2018 and 2019, we investigated 20 fundamental S_N2 reactions, X^- + CH_3Y [X = OH, SH, CN, NH_2, PH_2; Y = F, Cl, Br, I], with high-level *ab initio* methods characterizing the stationary points of the Walden-inversion, front-side attack and double-inversion pathways.[37,38] In 2020, we developed global analytical PESs for the OH^- + CH_3I reaction using various *ab initio* methods, which were the first full-dimensional PESs for a seven-atomic S_N2 reaction.[39] It turned out that at certain geometries, the CCSD(T)-F12b method fails by giving excessive negative energies due to the perturbative (T) approximation. To solve this issue, we suggested a composite *ab initio* method in which the (T) correlation is described by the more robust Brueckner coupled-cluster theory.[40]

In the present work, exceeding the OH^- + CH_3I/CH_3F seven-atomic systems,[33,39] we perform the first high-level dynamical characterization of a more challenging eight-atomic NH_2^- + CH_3I reaction. Utilizing the in-house ROBOSURFER program,[41] we develop a global analytical *ab initio* PES for the title reaction to compute more than half million full-length quasi-classical trajectories (QCT) at four different collision energies (E_{coll}). In addition to S_N2 and proton abstraction, significant iodine abstraction is uncovered leading to the CH_3 + $[NH_2\cdots I]^-$ products. Our dynamics simulations allow us to determine the configuration of the CH_3NH_2 products; thus, it is feasible to identify S_N2 reactions occurring with retention of the initial CH_3I configuration.[42] The simulation trajectories unveil two dominant novel retention pathways: complex formation and Walden inversion with complex formation. How do these mechanisms proceed and what is their key feature? How competitive the iodine abstraction compared to the S_N2 or proton abstraction and what other product channels can also be found? In the following, we provide a thorough dynamical description of the title reaction including the answers to the above questions.

COMPUTATIONAL DETAILS

The stationary points of the NH_2^- + CH_3I → CH_2I^- + NH_3 reaction are characterized using the second-order Møller–Plesset perturbation theory (MP2)[43] with the correlation-consistent aug-cc-pVDZ(-PP) basis set and the explicitly correlated coupled-cluster singles, doubles, and perturbative triples CCSD(T)-F12b method[44] with the aug-cc-pVDZ and aug-cc-pVTZ basis sets.[45] Then, the benchmark energies are obtained by utilizing the CCSD(T)-F12b method with the aug-cc-pVQZ basis set at the corresponding CCSD(T)-F12b/aug-cc-pVTZ geometries. The *ab initio* computations are performed using the MOLPRO program package.[46] The benchmark energies of the S_N2 stationary points are taken from Ref. 38.

The following step is to build a global, analytical PES for the title reaction using the ROBOSURFER program package developed recently in our group.[41] An initial dataset is constructed by (1) randomly modifying the Cartesian coordinates of the stationary points and (2) positioning the fragments of the reactants or products from each other in the range of 2.0–10.0 Å. The energies of the generated random geometries are obtained at the MP2/aug-cc-pVDZ level of theory; then, this dataset is applied to start the ROBOSURFER program for iterative improvement by selecting the remaining points derived from QCT calculations. Performing 90, 90, 64, and 18 iterations at 5, 10, 20, and 30 kcal/mol E_{coll} in an order, the dataset contains 26 978 energy points. For PES fitting, the permutationally invariant polynomial approach[47,48] is used with a fifth-order polynomial expansion of Morse-like variables, $\exp(-r_{ij}/a)$, where r_{ij} are the inter-atomic distances and a = 3 bohrs. 5419 polynomial coefficients are determined by a weighted linear least-squares fit applying the weight function of $E_0/(E + E_0) \times E_1/(E + E_1)$, where E_0 = 94 kcal/mol, E_1 = 314 kcal/mol, and E is the energy relative to the global minimum. As for the OH^- + CH_3I reaction,[39] the same CCSD(T)-F12b failure can be recognized: The gold-standard method breaks down at certain geometries; thus, the energy points are recalculated at the CCSD-F12b/aug-cc-pVTZ + BCCD(T)/aug-cc-pVDZ − BCCD/aug-cc-pVDZ[40] composite level of theory resulting 26 918 structures. For further improvement of the PES, ROBOSURFER is utilized at 5, 10, and 20 kcal/mol E_{coll} containing 47, 98, and 50 iterations, respectively, using the latter composite level of theory. The final PES consists of 31 840 energy points, and the root-mean-square errors of the fitting are 1.04, 1.68, and 2.37 kcal/mol for the energy ranges 0–94 kcal/mol, 94–188 kcal/mol, and 188–233 kcal/mol, in order.

QCT simulations are performed for the $NH_2^-(v = 0)$ + CH_3I (v = 0) reaction at 5, 10, 20, and 30 kcal/mol E_{coll} on the final analytical composite PES. The spatial orientations of the reactants are randomly sampled, and the initial distance of the reactants is 40 bohr with a given impact parameter (b). The vibrational ground states (v = 0) of NH_2^- and CH_3I are provided by standard normal-mode sampling and the rotational temperatures are set to 0 K. At each E_{coll}, b is scanned with the step size of 0.5 bohr from 0 to b_{max}, where the probability of the reaction becomes zero. At each b, 5000 trajectories are run using a time step of 0.0726 fs, and each trajectory is propagated until the largest interatomic distance becomes larger than the largest initial one by 1 bohr. Altogether, in the present study, more than half million trajectories are considered. For S_N2 and proton abstraction, different ZPE restrictions are considered: soft (discarding trajectories if the sum of the classical vibrational energy of the CH_2I^- and NH_3 products is less than the sum of their ZPEs on the present PES) and hard (discarding trajectories if the vibrational energy of either product is less than its ZPE on the present PES). The vector-projection method is used to identify the retention and inversion trajectories of the S_N2 channel.[42] The separation of the possible S_N2 retention pathways (front-side attack, double inversion, complex formation, and Walden inversion with complex formation) is carried out by evaluating the trajectories step by step.

A more detailed description of the calculations is presented in the supplementary material.

RESULTS AND DISCUSSION

The schematic PES of the NH_2^- + CH_3I S_N2 and proton abstraction is shown in Fig. 1 with the benchmark classical relative energies of the stationary points compared to the PES values. The S_N2 reaction is highly exothermic (−86.09 kcal/mol), and the back-side attack Walden inversion is barrierless, which can proceed via a hydrogen-bonded complex (HMIN, −16.34 kcal/mol) in the entrance channel, followed by a pre-reaction transition state (PreTS, −15.62 kcal/mol), where the orientation of the NH_2 unit differs from the other WaldenTSs of the NH_2^- + CH_3Y (Y = F, Cl) S_N2 reactions,[38] and then finally, a $I^-\cdots$ HNH–bonded global minimum complex (PostHMIN, −93.40 kcal/mol) is found in the exit channel. A stable front-side complex formation can be assessed:[18,36] FSMIN is below HMIN by 9.4 kcal/mol, while in the case of OH^- + CH_3I, this value is 5.2 kcal/mol.[37] Furthermore, this front-side complex formation may assist iodine abstraction resulting the CH_3 + $[NH_2\cdots I]^-$ products.[29] In addition to the traditional Walden inversion, retention can also occur: The transition state of the front-side attack (FSTS) has a barrier height of only 9.03 kcal/mol; moreover, double inversion has a submerged transition state (DITS, −11.70 kcal/mol). Proton abstraction is less exothermic than that of S_N2 with an energy of −16.77 kcal/mol, for which seven submerged stationary points are determined (three minima and four transition states). Note that the arrangement of the stationary points on the proton-abstraction schematic PES is based on our chemical intuition and the high similarity to the OH^- + CH_3I → CH_2I^- + H_2O reaction.[28] The relative energies of the stationary points obtained on the PES are in good agreement with the benchmark CCSD(T)-F12b/aug-cc-pVQZ energies, except for FSTS, where a difference of ~1.9 kcal/mol emerges.

To provide a detailed dynamical characterization of the NH_2^- + CH_3I reaction, QCT computations are performed at four different E_{coll} (5, 10, 20, and 30 kcal/mol) with a time step of 0.0726 fs. The details of the QCT calculations are presented in the supplementary material. For the title reaction, several different product channels are distinguished by evaluating the relevant atomic distances: S_N2 (CH_3NH_2 + I^-), proton abstraction (CH_2I^- + NH_3), iodine abstraction ($[NH_2\cdots I]^-$ + CH_3), S_N2 with rupture ($[CH_3\cdots NH_2]$ + I^-), and proton abstraction with rupture (CH_2 + I^- + NH_3). The difference of the products between S_N2 and S_N2 with rupture is the distance of the C and N atoms at the end of each trajectory: $d_{C-N} < 3.0$ Å for the former and $d_{C-N} > 3.0$ Å for the latter. The situation is the same for proton abstraction and proton abstraction with rupture: $d_{C-I} < 5.0$ Å and $d_{C-I} > 5.0$ Å, respectively. Since the five H atoms are labeled in a dynamics simulation, besides S_N2 retention pathways, we can also determine S_N2 reactions taking place with a proton exchange between the CH_3I and NH_2^- reactants preceding the traditional Walden inversion.

The integral cross sections (ICSs) as a function of E_{coll} for the above-mentioned reaction routes are presented in Fig. 2 and Table S1. Since S_N2 and proton abstraction are exothermic and

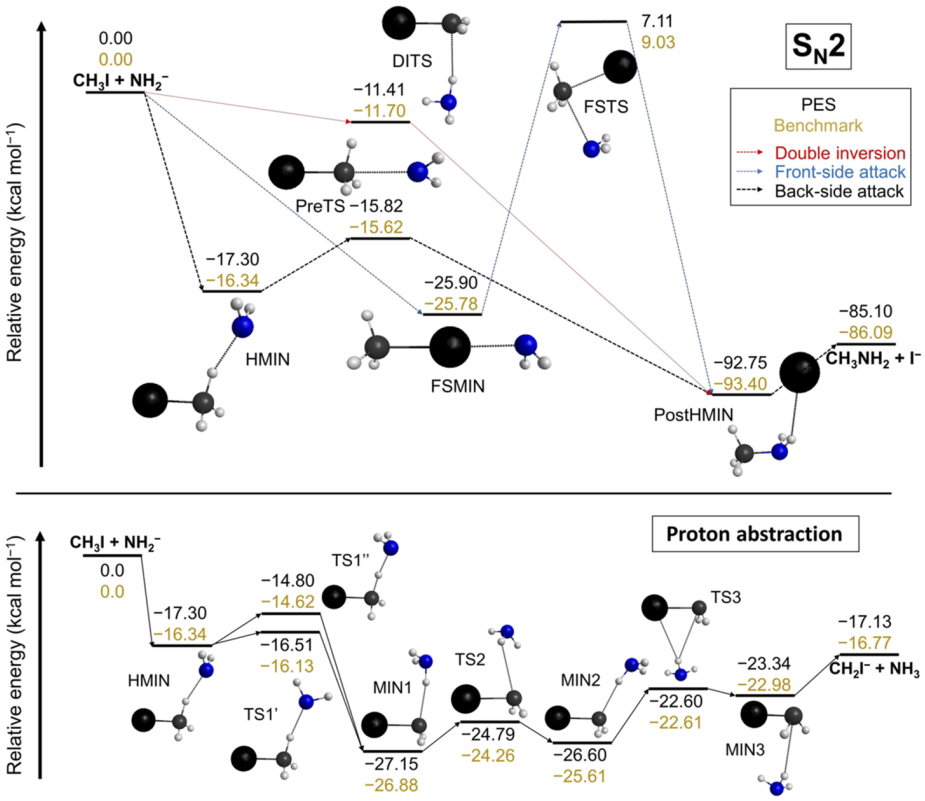

FIG. 1. Schematic potential energy surfaces of the NH_2^- + CH_3I S_N2 and proton-abstraction reactions showing the stationary points along different pathways with the benchmark classical relative energies compared to the PES values. For the S_N2 pathway, the benchmark data are adapted from Ref. 38.

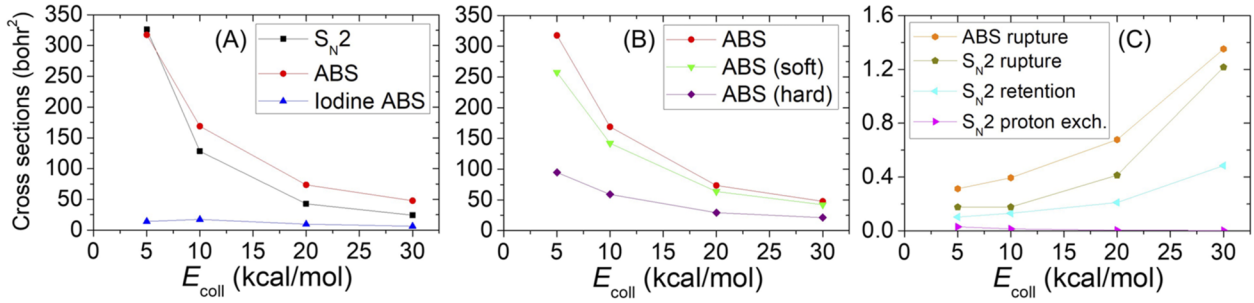

FIG. 2. Integral cross sections for (a) S_N2, proton abstraction, and iodine abstraction; (b) proton abstraction with soft and hard ZPE restrictions; and (c) proton abstraction with rupture, S_N2 with rupture, S_N2 with retention, and S_N2 with proton exchange pathways of the NH_2^- + CH_3I reaction as a function of collision energy. For the details of the ZPE constraints, see the section entitled as "Computational details."

barrier–less reactions, the ICSs of these pathways decrease as the E_{coll} increases. In contrast, iodine abstraction ICS peaks at E_{coll} = 10 kcal/mol with a value of ~17 bohr^2 and then decreases with increasing E_{coll}. As the decrease of the S_N2 and proton-abstraction ICSs is steeper than in the case of iodine abstraction, at high E_{coll}, iodine abstraction becomes relatively more and more competitive. For S_N2 and proton abstraction, we consider zero-point energy (ZPE) violations of the products as well. Using hard ZPE constraint, the ICS of the proton abstraction significantly drops, while for S_N2, the restriction is ineffective, as expected for an extremely exothermic reaction; therefore, it becomes the most dominant pathway for the title reaction. At each E_{coll}, the possibility of proton abstraction with rupture is higher than that of S_N2 with rupture, and their ICSs are increasing with E_{coll}. S_N2 with proton exchange has the smallest ICSs with a maximum of ~0.03 bohr^2 at E_{coll} = 5 kcal/mol and almost vanishes at higher E_{coll}. Considering the retention pathways, as expected, the possibility increases with E_{coll}: An ICS of ~0.48 bohr^2 is determined at E_{coll} = 30 kcal/mol.

For the products of S_N2 and proton abstraction, the relative translational and internal energy distributions and the scattering angle distributions as well, are shown in Fig. 3–5, respectively. The direct pathway of the proton abstraction becomes more and more significant as E_{coll} raises: The translational energy distributions of the CH_2I^- + NH_3 products depend on E_{coll}, while in case of the internal energies, no dependence can be assigned. For S_N2, the tendency of the product energy distributions is reversed; with increasing E_{coll}, the internal energies of the products are more impacted than the translational energies, indicating a vibrationally excited CH_3NH_2 product. These findings are also confirmed by the scattering angle distributions: The forward-scattered products of the proton abstraction propose a dominance of the direct stripping mechanism; however, for S_N2 at high E_{coll}, a near–isotropic profile can be identified suggesting a relatively indirect reaction pathway. In Fig. S1, the average integration time of S_N2, proton, and iodine abstractions are depicted at each E_{coll}, from b = 0–6 or 9 bohr, depending on the statistical representativeness of the iodine abstraction. For proton and iodine abstractions, the average time of the trajectories decreases at each b with increasing E_{coll}. In contrast, for S_N2 at small b, the average integration time peaks at E_{coll} = 10 kcal/mol, while at large b, a decrease can be assessed. Thus, S_N2 becomes the slowest reaction pathway at small b as E_{coll} increases.

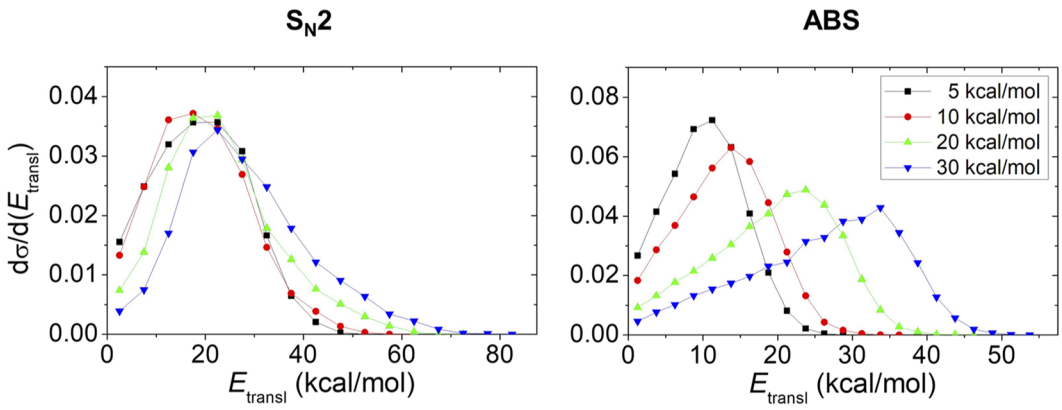

FIG. 3. Relative translational energy distributions of the products of S_N2 (CH_3NH_2 + I^-) and proton abstraction (CH_2I^- + NH_3) for the NH_2^- + CH_3I reaction at different collision energies.

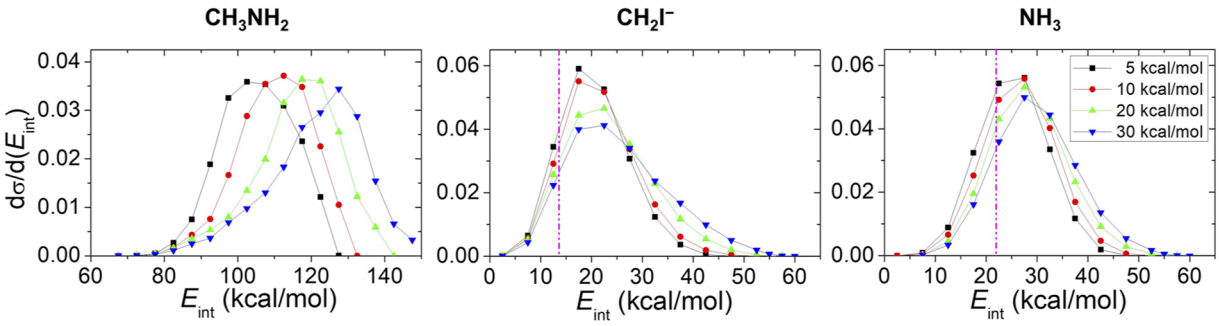

FIG. 4. Relative internal energy distributions of the products of S_N2 (CH_3NH_2) and proton abstraction (CH_2I^- + NH_3) for the NH_2^- + CH_3I reaction at different collision energies. The purple vertical dotted line refers to the zero-point energies of the CH_2I^- (13.60 kcal/mol) and NH_3 (21.97 kcal/mol) products on the present PES. For S_N2, the zero-point energy of CH_3NH_2 is 40.59 kcal/mol; thus, no product ZPE violation can be determined.

Looking into the possible mechanisms of the retention pathways, we can describe the indirect nature of the NH_2^- + CH_3I S_N2 reaction. Due to the long-range ion-dipole interactions of the CH_3I and NH_2^- reactants, the system is more and more vibrationally excited with increasing E_{coll}, supporting the formations of the $[CH_3\cdots NH_2]$, $[NH_2\cdots I]^-$, or $[CH_2\cdots I]^-$ complexes as a result of the C–I bond rupture in CH_3I. The generation of the $[NH_2\cdots I]^-$, $[CH_2\cdots I]^-$ complexes promotes iodine abstraction and proton abstraction with rupture, respectively. In Fig. 6, the two unusual retention pathways are depicted for the title S_N2 reaction. As CH_3I and NH_2^- approach each other in a random orientation, the collision of the reactants induces the rupture of the C–I bond in CH_3I, and a $[CH_3\cdots NH_2]$ complex is formed. Simultaneously, a significant energy transfer occurs: The translational energy converts to internal energy; thus, the fragments of the $[CH_3\cdots NH_2]$ complex become vibrationally and rotationally highly excited. For the formation of the CH_3NH_2 final product, an optimal relative orientation of the CH_3 and NH_2 fragments is required due to the numerous repulsive interactions between the polyatomic fragments. Hence, in some cases, these hot $[CH_3\cdots NH_2]$ complexes result in the final CH_3NH_2 retention product by the cause of the rotation of the CH_3 fragment. On the other hand, the inverted highly excited product of the Walden inversion may lead to the generation of the $[CH_3\cdots NH_2]$ complex, and as the CH_3 fragment turns around, the trajectory results in the double-inverted CH_3NH_2 product. It should be noted that this latter pathway was uncovered for the F^- + CH_3Br S_N2 reaction as well,[49] but a smaller ICS was determined with a short-lived complex formation. The direct *ab initio* potential energies are compared with the fitted PES values for the representative trajectories of the complex formation and Walden inversion with complex formation in Figs. S3 and S4, respectively. As it can be seen, the direct composite *ab initio* energies and the PES values are in good agreement, and no irregular deep well appears for the PES, although in certain regions, the *ab initio* energies are not obtained due to the convergence problems of the coupled-cluster method. This may create a slight uncertainty in our results; however, this issue is not uncommon: In these regions, the *ab initio* computations can be highly sensitive to the applied level of theory. The similar situation occurred for the OH^- + CH_3I reaction,[39] and the detailed *ab initio* investigation revealed that the currently

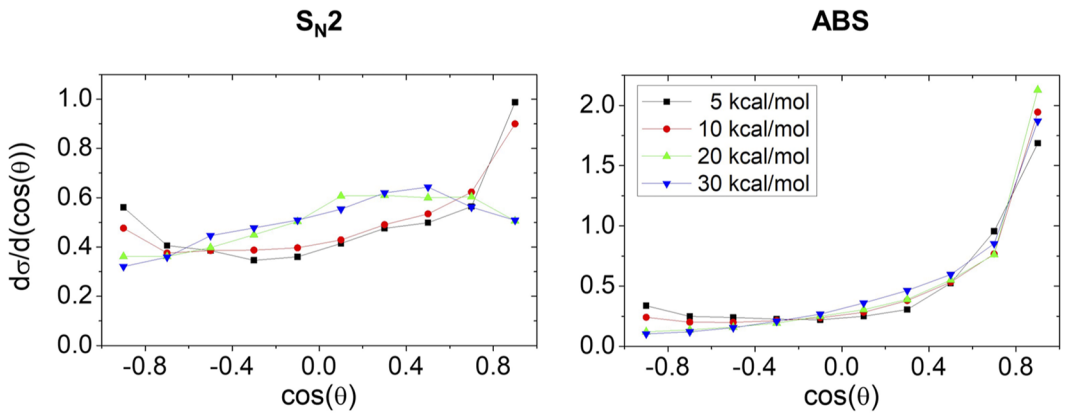

FIG. 5. Normalized scattering angle distributions of the NH_2^- + CH_3I reaction for S_N2 and proton abstraction at different collision energies.

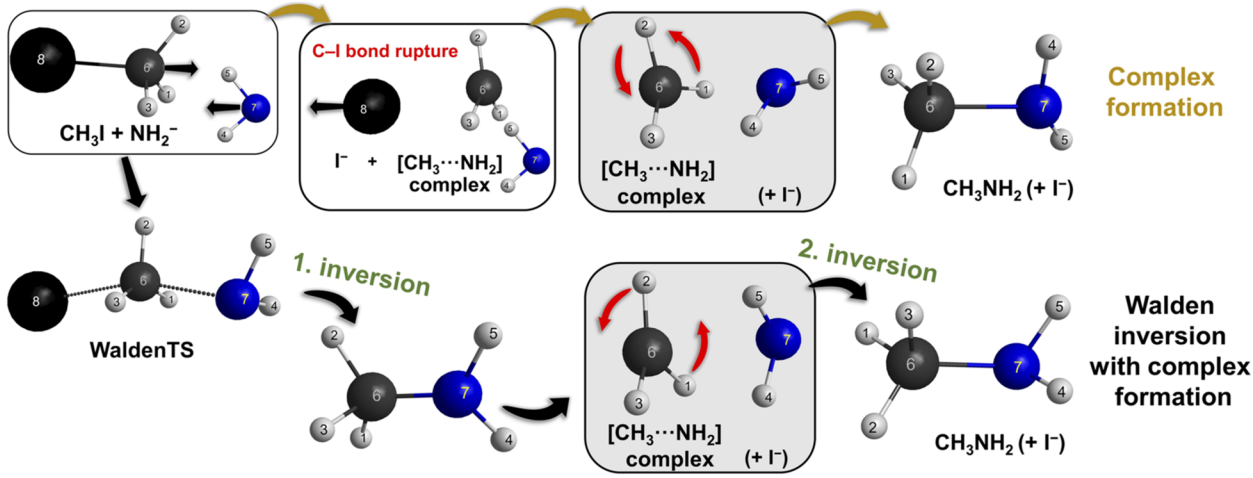

FIG. 6. Snapshots of the novel S_N2 retention mechanisms (complex formation and Walden inversion with complex formation) for the NH_2^- + CH_3I reaction. In both mechanisms, highlighted by gray background, the crucial feature is the formation of the $[CH_3\cdots NH_2]$ complexes in which a rotation of the CH_3 group can occur. As the labeling of the H atoms demonstrates, the simulation trajectories result in the CH_3NH_2 products with a retention of the CH_3I reactant configuration.

utilized composite level of theory is the most suitable for PES developments. In the supplementary material, QCT simulations for the novel retention pathways can be found in motion along with the other (direct/indirect S_N2 inversion, proton abstraction, iodine substitution, etc.) pathways. In Fig. 7 and Table S2, the ICSs of the S_N2 retention pathways are shown for the NH_2^- + CH_3I reaction at E_{coll} = 20 and 30 kcal/mol. As it can be seen at each E_{coll}, complex formation is the most favorable retention pathway. The ICS of the Walden inversion with complex formation has a maximum of ~0.15 $bohr^2$; however, despite the relatively low barrier height of FSTS, the front-side attack is the less possible path with an ICS of only ~0.03 $bohr^2$ at E_{coll} = 30 kcal/mol, presuming that the formation of the $[CH_3\cdots NH_2]$ complex inhibits the front-side attack mechanism. It is also notable that the typical double-inversion mechanism does not occur in the title reaction: Following the $CH_2H'I$ + NH_2^- → CH_2I^- + NH_2H' proton abstraction, instead of H'^+, a different H^+ transfers to CH_2I^- from NH_2H', and afterward, the traditional Walden inversion results in the S_N2 proton exchange products (CH_3NHH' + I^-).

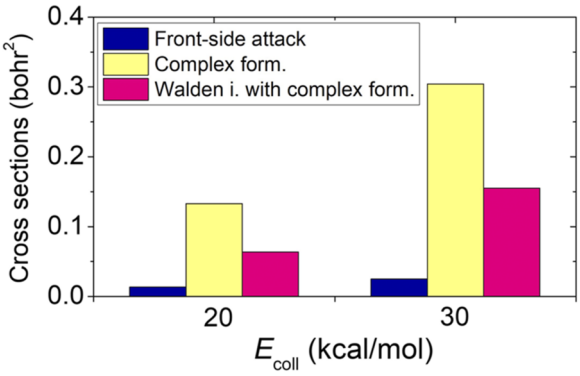

FIG. 7. Integral cross sections of the possible S_N2 retention pathways (front-side attack, complex formation, and Walden inversion with complex formation) for the NH_2^- + CH_3I reaction at the collision energies of 20 and 30 kcal/mol.

CONCLUSIONS

In light of our results, by increasing the complexity of the chemical reactions, novel mechanisms can be identified with an unusual feature. In the case of the NH_2^- + CH_3I reaction, two unexpected retention mechanisms are unveiled for the S_N2 pathway. At higher E_{coll}, an indirect nature of the S_N2 is identified inducing the formation of the $[CH_3\cdots NH_2]$ complexes. The key of these novel retention pathways is the rotation of the CH_3 fragment in the $[CH_3\cdots NH_2]$ complexes. We assume that these novel retention pathways may also occur in other polyatomic X^- + CH_3Y S_N2 reactions, such as X = PH_2, CH_3, SiH_3, HOO, HSO, and CH_3O for Y = F, Cl, Br, and I.[8] Furthermore, compared to the OH^- + CH_3I reaction,[29] a more significant iodine abstraction is uncovered leading to the CH_3 + $[NH_2\cdots I]^-$ products. We hope that our findings of the title reaction encourage further theoretical and experimental studies on more complex chemical reactions.

SUPPLEMENTARY MATERIAL

See the supplementary material for computational details, the integral cross sections of the studied pathways [S_N2 inversion, proton abstraction (with ZPE-constraints), iodine substitution, proton abstraction with rupture, S_N2 with rupture, S_N2 retention (complex formation, Walden inversion with complex formation, and front-side attack), and S_N2 with proton exchange], the

average integration time of the S_N2, proton-abstraction and iodine-abstraction pathways, opacity functions of the S_N2, proton abstraction and iodine abstraction pathways, comparison of direct *ab initio* energies and fitted PES values for two representative retention trajectories, benchmark Cartesian coordinates (Å) and energies (E_h) of the stationary points, representative trajectories of the reaction pathways, and codes for PES evaluation (Ref. 47).

ACKNOWLEDGMENTS

We thank the National Research, Development and Innovation Office–NKFIH, Grant No. K-125317; the Ministry of Human Capacities, Hungary, Grant No. 20391-3/2018/FEKUSTRAT; Project No. TKP2021-NVA-19, provided by the Ministry of Innovation and Technology of Hungary from the National Research, Development and Innovation Fund, financed under the TKP2021-NVA funding scheme; the National Young Talent Scholarship (Grant No. NTP-NFTÖ-21-B-0195 for D.A.T.); and the Momentum (Lendület) Program of the Hungarian Academy of Sciences for their financial support. The authors thank Dr. Bastiaan Braams for giving them permission to share the PES libraries as supplementary material.

AUTHOR DECLARATIONS

Conflict of Interest

The authors have no conflicts to disclose.

DATA AVAILABILITY

The data that support the findings of this study are available from the corresponding authors upon reasonable request.

REFERENCES

[1] C. K. Ingold, *Structure and Mechanism in Organic Chemistry* (Cornell University Press, Ithaca, NY, 1953).
[2] A. Streitwieser, Chem. Rev. **56**, 571 (1956).
[3] W. L. Hase, Science **266**, 998 (1994).
[4] M. L. Chabinyc, S. L. Craig, C. K. Regan, and J. I. Brauman, Science **279**, 1882 (1998).
[5] J. M. Gonzales, C. Pak, R. S. Cox, W. D. Allen, H. F. Schaefer III, A. G. Császár, and G. Tarczay, Chem. - Eur. J. **9**, 2173 (2003).
[6] J. Mikosch, S. Trippel, C. Eichhorn, R. Otto, U. Lourderaj, J. X. Zhang, W. L. Hase, M. Weidemüller, and R. Wester, Science **319**, 183 (2008).
[7] R. Otto, J. Brox, S. Trippel, M. Stei, T. Best, and R. Wester, Nat. Chem. **4**, 534 (2012).
[8] T. A. Hamlin, M. Swart, and F. M. Bickelhaupt, ChemPhysChem **19**, 1315 (2018).
[9] R. Wester, Mass Spectrom. Rev. (Published online 2021).
[10] R. H. Bathgate and E. A. Moelwyn-Hughes, J. Chem. Soc. **0**, 2642 (1959).
[11] F. G. Bordwell and W. T. Brannen, J. Am. Chem. Soc. **86**, 4645 (1964).
[12] A. Dedieu and A. Veillard, Chem. Phys. Lett. **5**, 328 (1970).
[13] A. Dedieu and A. Veillard, J. Am. Chem. Soc. **94**, 6730 (1972).
[14] H. B. Schlegel, K. Mislow, F. Bernardi, and A. Bottoni, Theor. Chim. Acta **44**, 245 (1977).
[15] W. N. Olmstead and J. I. Brauman, J. Am. Chem. Soc. **99**, 4219 (1977).
[16] S. S. Shaik, J. Am. Chem. Soc. **106**, 1227 (1984).
[17] J. Chandrasekhar, S. F. Smith, and W. L. Jorgensen, J. Am. Chem. Soc. **107**, 154 (1985).
[18] J. Xie and W. L. Hase, Science **352**, 32 (2016).
[19] I. Szabó and G. Czakó, J. Phys. Chem. A **121**, 9005 (2017).
[20] I. Szabó and G. Czakó, Nat. Commun. **6**, 5972 (2015).
[21] L. Sun, K. Song, and W. L. Hase, Science **296**, 875 (2002).
[22] L. Sun, K. Song, W. L. Hase, M. Sena, and J. M. Riveros, Int. J. Mass Spectrom. **227**, 315 (2003).
[23] T. Tsutsumi, Y. Ono, Z. Arai, and T. Taketsugu, J. Chem. Theory Comput. **16**, 4029 (2020).
[24] H. Tachikawa, M. Igarashi, and T. Ishibashi, J. Phys. Chem. A **106**, 10977 (2002).
[25] H. Tachikawa and M. Igarashi, Chem. Phys. **324**, 639 (2006).
[26] H. Yin, D. Wang, and M. Valiev, J. Phys. Chem. A **115**, 12047 (2011).
[27] Y. Xu, T. Wang, and D. Wang, J. Chem. Phys. **137**, 184501 (2012).
[28] J. Xie, S. C. Kohale, W. L. Hase, S. G. Ard, J. J. Melko, N. S. Shuman, and A. A. Viggiano, J. Phys. Chem. A **117**, 14019 (2013).
[29] J. Xie, R. Sun, M. R. Siebert, R. Otto, R. Wester, and W. L. Hase, J. Phys. Chem. A **117**, 7162 (2013).
[30] J. Xie, R. Otto, J. Mikosch, J. Zhang, R. Wester, and W. L. Hase, Acc. Chem. Res. **47**, 2960 (2014).
[31] J. Chen, Y. Xu, and D. Wang, J. Comput. Chem. **35**, 445 (2014).
[32] Y. G. Proenza, M. A. F. de Souza, and R. L. Longo, Chem. - Eur. J. **22**, 16220 (2016).
[33] D. A. Tasi and G. Czakó, Chem. Sci. **12**, 14369 (2021).
[34] J. Xie, J. Zhang, and W. L. Hase, Int. J. Mass Spectrom. **378**, 14 (2015).
[35] J. Xie, J. Zhang, R. Sun, R. Wester, and W. L. Hase, Int. J. Mass Spectrom. **438**, 115 (2019).
[36] X. Ji, C. Zhao, and J. Xie, Phys. Chem. Chem. Phys. **23**, 6349 (2021).
[37] D. A. Tasi, Z. Fábián, and G. Czakó, J. Phys. Chem. A **122**, 5773 (2018).
[38] D. A. Tasi, Z. Fábián, and G. Czakó, Phys. Chem. Chem. Phys. **21**, 7924 (2019).
[39] D. A. Tasi, T. Győri, and G. Czakó, Phys. Chem. Chem. Phys. **22**, 3775 (2020).
[40] K. A. Brueckner, Phys. Rev. **96**, 508 (1954).
[41] T. Győri and G. Czakó, J. Chem. Theory Comput. **16**, 51 (2020).
[42] P. Papp, V. Tajti, and G. Czakó, Chem. Phys. Lett. **755**, 137780 (2020).
[43] C. Møller and M. S. Plesset, Phys. Rev. **46**, 618 (1934).
[44] T. B. Adler, G. Knizia, and H.-J. Werner, J. Chem. Phys. **127**, 221106 (2007).
[45] T. H. Dunning, J. Chem. Phys. **90**, 1007 (1989).
[46] H.-J. Werner, P. J. Knowles, G. Knizia, F. R. Manby, and M. Schütz *et al.*, MOLPRO, version 2015.1, a package *ab initio* programs, see http://www.molpro.net.
[47] B. J. Braams and J. M. Bowman, Int. Rev. Phys. Chem. **28**, 577 (2009).
[48] J. M. Bowman, G. Czakó, and B. Fu, Phys. Chem. Chem. Phys. **13**, 8094 (2011).
[49] V. Tajti, T. Győri, and G. Czakó, J. Chem. Phys. **155**, 124301 (2021).